ACS SENSORS

pubs.acs.org/acssensors

Article

Micromotor-Based Biosensing Using Directed Transport of Functionalized Beads

Sinwook Park and Gilad Yossifon*

Cite This: *ACS Sens.* 2020, 5, 936−942

Read Online

ACCESS | Metrics & More | Article Recommendations | Supporting Information

ABSTRACT: Previous micromotor-based biosensing studies used to functionalize the surface of the micromotor with specific molecular probes for binding of target analyte, thus limiting the use of the micromotor for the specific target. In contrast, here, we introduce a novel approach of using a nonfunctionalized micromotor as a generic cargo carrier being able to perform label-free and dynamic loading, transport, and release of functionalized beads. Hence, such an approach enables one to use the same micromotor system for sensing of varying targets via different commercially available functionalized beads, demonstrating the use of micromotors as a practical and versatile means for biosensing. We have also introduced a simplified microfluidic design that can be used for immunosensing or DNA binding tests without necessity for complicated fluid handling (buffer exchange, washing, etc.) steps. We expect this approach to open up new realizations of simplified and generic biosensing platforms.

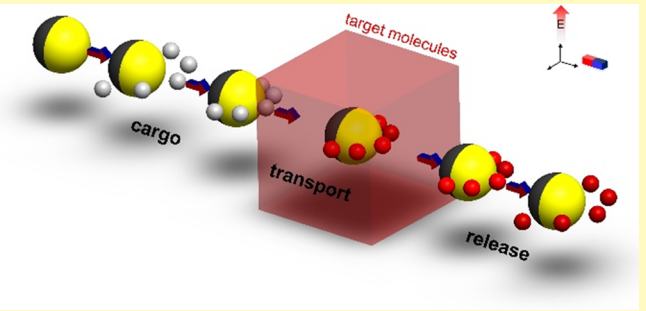

KEYWORDS: *micromotor-based biosensing, active carrier, self-propelling particle, Janus particle, dielectrophoresis, ICEP*

The reliable identification of the target analytes using lab-on-a-chip technology promises an enormous potential in the fields of environmental monitoring, food testing, food/water safety monitoring, and clinical analysis.[1] In particular, the emerging field of self-propulsion (i.e., "active" particles) combined with microfluidics offers new opportunities for realization of novel micromotor-based biosensing, targeted drug delivery, and cell manipulation/isolation for biomedical application.[2−7] Active particles that convert energy at the particle level from the surrounding environment (e.g., chemical fuel,[8−11] light,[12,13] ultrasound,[14] magnetic field,[15−18] and electric field[19−21]) into autonomous self-propulsion enables efficient coverage of large areas and volumes while operating under uniform ambient conditions without the need to generate field gradients for driving the particles.

By using different materials and surface coating techniques (e.g., molecularly imprinted polymers,[8,22] biodegradable and biocompatible polymers,[23] and biomimetic material[24]), the active particles coated with biodegradable materials or functionalized with bioreceptors have been proven to be useful for various tasks such as antibacterial activity,[23] protein detection,[25] and intracellular biosensing of a target miRNA expressed in intact cancer cells.[26] As one notable approach, García et al.[8] demonstrated micromotor-based immunoassay using self-propelled antibody-functionalized micromotors where the different immunoassay steps are obtained via the mobile particle translating between different reservoirs connected using microfluidic channels. This concept eliminates the need to manipulate fluids as common to lab-on-a-chip devices; thus, the washing step is obtained by the motion of the particle itself within the stagnant fluid. However, the coating of the active particle with antibodies makes these micromotors specific and less generic in application.

Here, we demonstrate a generic approach using a nonlabeled micromotor that can selectively load, transport, and release functionalized beads (i.e., treated as cargo) singularly controlled by an external alternating electric field. We use spherical metallodielectric Janus particle (JPs) as the micromotor,[19,21,27,28] where under an applied electric field, the imbalanced polarization at metallic and dielectric hemispheres results in self-propulsive behavior referred to induced-charge electrophoresis (ICEP)[29,30] and self-dielectrophoresis (sDEP).[19] Both the speed and direction of the JP are controlled by the applied electric field frequency, with the JP propelling either with its dielectric (ICEP) or metallic (sDEP) hemisphere forward.[19,28,29]

The underlying mechanism of the cargo manipulation used in the current work is dielectrophoresis (DEP), which enables label-free loading and release of a broad range of organic and inorganic cargos.[20] Under a uniform external electric field, the

Received: October 17, 2019
Accepted: March 6, 2020
Published: March 6, 2020

field gradients, necessary for DEP force, are induced at the JP level. By varying the electric field frequency, a cargo particle can shift between attraction (i.e., positive DEP, pDEP) and repulsion (i.e., negative DEP, nDEP) at regions of high electric field intensity according to its geometry and material properties.[31−33] Thus, combining an electrically powered micromotor and DEP-based cargo manipulation enables us to use a uniform electric field to singularly control the selective loading, transport, and release of the functionalized beads in a simple and robust manner. Adding magnetic steering, using a ferromagnetic coating of the JPs with an externally rotating static magnet, enabled us also to precisely navigate the micromotor.[34−36]

Here, we present micromotor-based biosensing using simplified microfluidic devices consisting of either a single chamber (Figure 3) or two chambers with connecting microchannel (Figure 5). As described in the schematics in Figure 1, the micromotor first loads the functionalized beads as

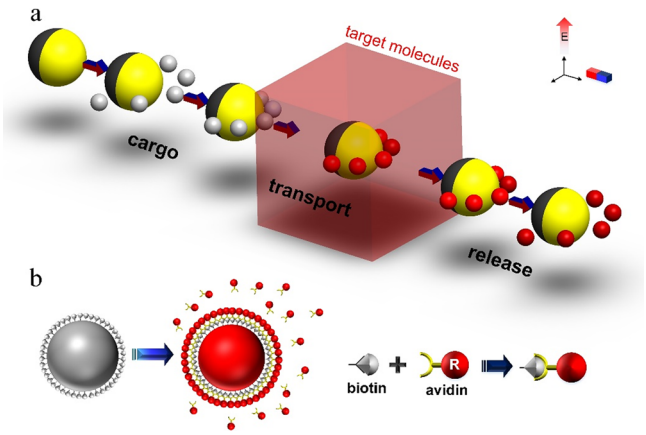

Figure 1. Schematic illustration of the concept of micromotor-based biosensing by cargo manipulation and transport of functionalized beads. (a) A Janus particle picks up biotin-functionalized beads and transports them to selected regions. An electric field is used for both JP propulsion and cargo manipulation (negative DEP trapping), while a magnetic field is used for steering of the JP. The metallic coated (Cr/Ni/Au) is colored yellow, while the nonfluorescent bare polystyrene hemisphere is colored dark gray. The red- and gray-colored cargos indicate the biotin-functionalized particles with and without avidin-biotin binding, respectively. (b) Biotin-avidin reactions are used as a simplified model of immunosensing and DNA biosensing, wherein the biotin-coated beads bind to avidin molecules that are introduced into the sample solution.

cargos and then transports them toward the sample of the target analyte for some certain incubation time for its "on-the-fly" binding with specific molecular probes that are functionalized on the surface of the beads. This is followed by a washing step wherein the beads are transported into a region free of the target analyte for visualization of the binding before release. The micromotor can be reused to load and transport new cargos following release of the previously transported cargos. Without loss of generality, we used biotin-avidin with high affinity as a simplified model for immunosensing or protein and nucleic acid detection. While micromotor-based cargo loading was previously studied,[20,35,36] herein, we investigate for the first time its applicability for biosensing using commercially available functionalized microbeads. This involves consideration of the diffusion of the analyte within the microfluidic chamber and the dependency of the bimolecular binding between the target analyte and surface-immobilized probes on the analyte concentration as well as the retention time within the region where the analyte is introduced.

RESULTS AND DISCUSSION

Cargo Loading and Transport. Here, we characterized the cargo (biotin-coated beads) manipulation (i.e., loading, transport, and release). A 10 μm-diameter Ni-Au-coated Janus particle was used as a micromotor within an indium tin oxide (ITO)-sandwiched microchamber wherein the bottom ITO-coated glass slide was covered with thin silicon dioxide layer to suppress adsorption of particles onto the substrate[27] (more details are given in the Supporting Information). In particular, we examined the effect of the conductivity of a phosphate-buffered saline (PBS) solution on the micromotor velocity (Figure 2b and Figure S1). As shown, the electrokinetic propulsion of the JP becomes ineffective at high solution conductivities (>1 mS/cm; see Figure S1). The chosen solution conductivity at which we performed the study was 0.01% (v/v) PBS at which the JPs move fast enough (Figure 2b and Figure S1) to shorten the translocation time between the different regions but also enable sufficiently strong biotin-avidin binding affinity.

As shown in Figure 2a,b, there are two modes of self-propulsion, where the JP moves with its dielectric end forward under induced-charge electrophoresis (ICEP) at low frequencies and with its metallic end forward (sDEP) beyond a certain critical frequency. Also, the applied electric field frequency affects the dielectrophoretic response of the cargos, which transitions from pDEP to nDEP response with increasing frequency beyond the crossover frequency (COF) ∼10 kHz (Figure 2b).

Here, we chose to use the sDEP propulsion mode with nDEP cargo trapping (500 kHz) due to the larger cargo loading capacity (there is less hydrodynamic shear since electroconvection is significantly reduced at such high frequencies) and the relatively large carrier mobility. At lower frequency (5 kHz) with ICEP propulsion and pDEP cargo trapping mode, the cargos were trapped only at the top of the JP (see simulation inset in Figure 2d) due to its inability to penetrate underneath the JP due to size limitation but transported with a nonsmooth motion due to abrupt stops as a result of the loaded cargo (Figure S1). At the mode of sDEP and nDEP cargo trapping, the micromotor with magnetic steering is directed to capture functionalized beads in a consecutive manner with particles trapped on the equator of its metallic hemisphere, as seen in (Figure 2c, schematic inset in Figure 2d, and Supplementary Video S1). Figure 2d depicts how the increased number of loaded cargo is decreasing the mobility of the micromotor. This can be simply explained due to the increased Stokes drag resulting from the enlarged areal cross section of the loaded carrier due to the trapped cargos.[35,36] The maximal cargo loading capacity the micromotor is able to pick up was ∼7 for the current operating conditions. However, the maximal loading capacity can be changed depending on the JP size and operating conditions (Figure S2, Figure S3, and Supplementary Video S2).

A Single Microfluidic Chamber Setup. Here, we demonstrate our novel approach using a very simplified microfluidic setup consisting of a single chamber made of a spacer and two drilled inlet holes for introduction of the solution, functionalized beads, micromotor, and sample analyte (Figure 3). We can qualitatively differentiate between several

https://dx.doi.org/10.1021/acssensors.9b02041
ACS Sens. 2020, 5, 936−942

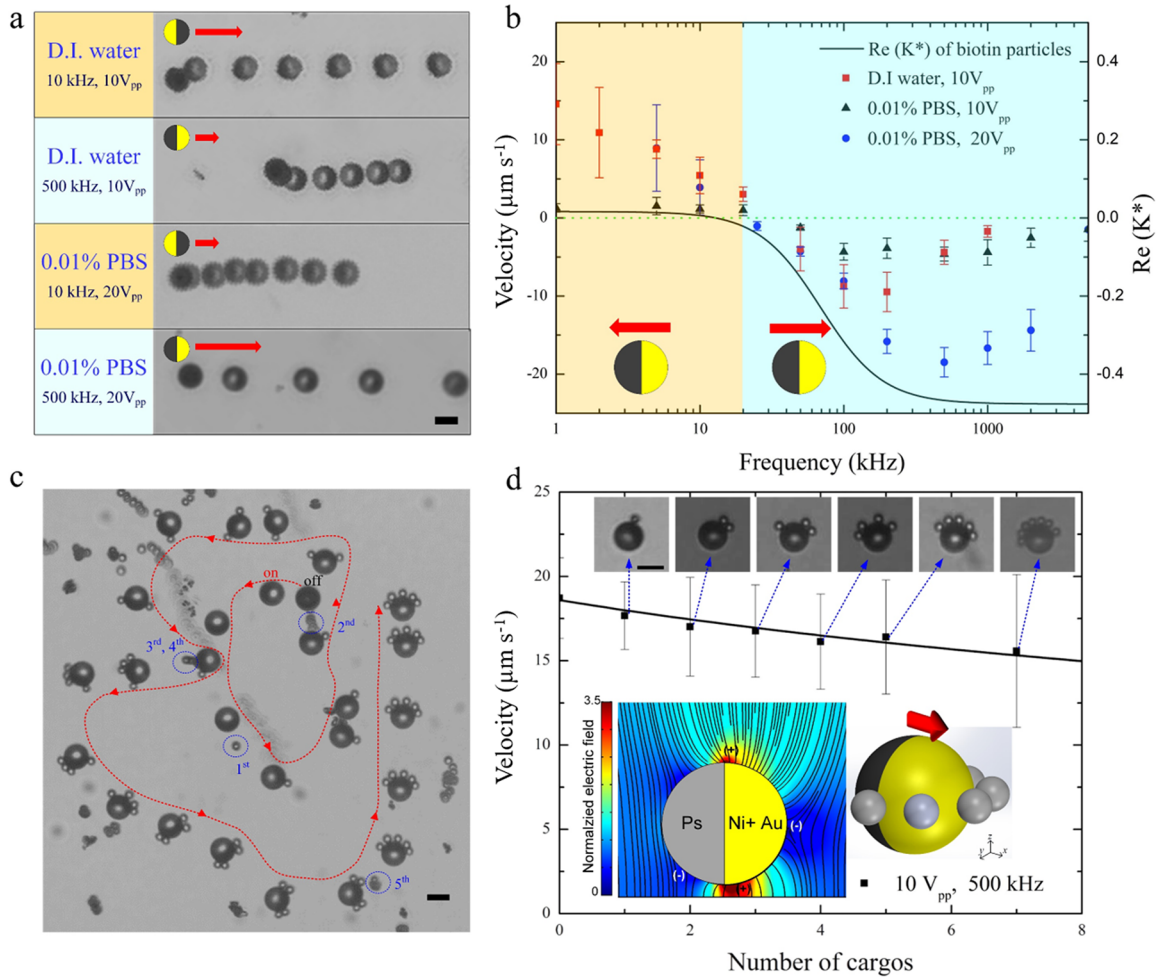

Figure 2. Characterization of self-propulsion of Janus particle and cargo transport of biotin-coated particles. (a) Superimposed sequential microscopy images showing the transport of 10 μm (in diameter) Cr/Ni/Au-coated Janus particle suspended in deionized (D.I.) water and 0.01% diluted PBS with conductivity (σ = 180 μS cm^{-1}). The JP motion is due to ICEP (polystyrene (PS) hemisphere forward) and sDEP (Au hemisphere forward) at electric field frequencies of 10 and 500 kHz, respectively. The red arrows indicate the direction of motion of the JP, and the time interval between superimposed images is 2 s. (b) Frequency dispersion of the Janus particle mobility at various solutions. The black line indicates the Clausius−Mossotti (CM) factor of a 3.5 μm (in diameter) biotin-coated particles (cargos) in 0.01% PBS (σ = 180 μS cm^{-1}) as extracted from their DEP response. (c) Superimposed images showing the pickup process of cargos by a single JP suspended in 0.01% diluted PBS. The applied electric field is 500 kHz and 20 V$_{pp}$, which results in sDEP-dominated JP propulsion and nDEP-trapped cargos that assemble on the equator of the JP (see Supplementary Video S1). The red arrow indicates the direction of the JP steered by magnetic force. (d) Carrier velocity vs the number of cargos under the electric field of 500 kHz and 10 V$_{pp}$. The bottom insets depict the distribution of the electric field around the JP, as obtained from the numerical simulations and corresponding locations where positive and negative DEP trapping of cargo can occur. Microscopy images in the insets depict varying number of nDEP-trapped cargos. Scale bars: 10 μm.

zones in between one of the inlets where the target sample analyte is gently introduced and the other inlet which is free of target analyte. Note that the distance between the two holes (~6.5 mm) is far enough for the target analyte not to reach the other inlet by diffusion during the whole process (~180 h with an avidin molecule diffusion coefficient of $D \approx 6.5 \times 10^{-7}$ cm^2 s^{-1}[37]). The micromotors and cargos (i.e., functionalized beads) were first introduced uniformly within the chamber before introducing the target analyte, although they could be as well introduced only into the inlet far from the analyte after filling the chamber with the solution. We have then used the micromotor to trap the cargos to follow a path along the avidin molecule concentration gradients for binding followed by a washing step. The binding of avidin molecules to the biotin-coated beads did not seem to change their DEP behavior in a way that necessitates readjustment of the operating parameters. The time of incubation can be then controlled by either increasing the retention time of the micromotor with loaded cargos within region I of the highest avidin concentration or simply picking up the beads within region I after some desired time (see Figure 4). As seen in Figure 3b, a clear binding event occurred between the avidin and the biotin-coated cargos following an incubation time of ~5 min. This shortened detection time, relative to the long diffusion time of avidin within the chamber, is clearly due to motion of the trapped cargos, via the micromotor, to the region of high analyte concentration. This is further quantified using different avidin concentrations to test the limit of detection of the system, which proves that, for two cycles, concentration as low as 2 μg/mL can be detected. It is expected that this can be further improved by simply increasing the incubation time (Figure 4c). As a control, we have used non-biotin-coated micro-particles of the same size, which showed no fluorescence signal

https://dx.doi.org/10.1021/acssensors.9b02041
ACS Sens. 2020, 5, 936−942

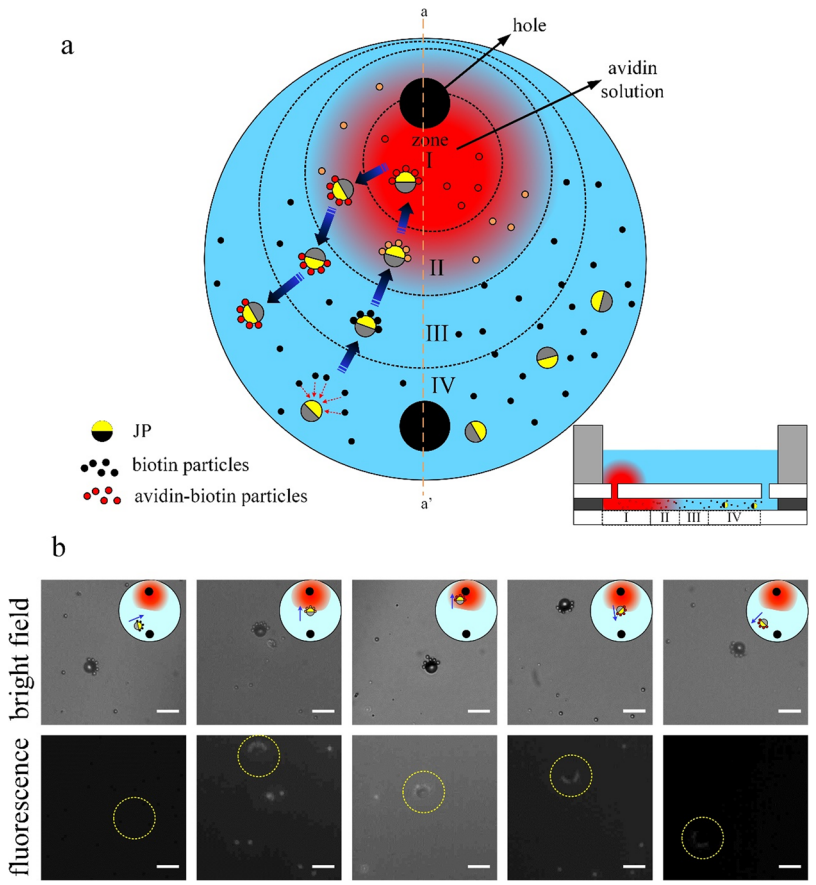

Figure 3. Transport of biotin-functionalized cargos using a micromotor for sensing of avidin within a single chamber system. (a) Schematics of the biosensing procedure including (i) micromotor loading several cargos while transporting them from zone IV to zone I for binding with avidin, (ii) incubation time of 5 min, and (iii) transport of cargo to the avidin-free region (zones I to IV) for washing nonspecifically bound molecules and detection of avidin-biotin binding. The inset depicts the cross-sectional side view of the system along the orange dashed line a–a′. (b) Time-lapse microscopy bright field (top row) and fluorescence (second row) images showing the micromotor-based transport of cargos across the different zones. The applied electric field is 500 kHz and 10 V_{pp} with sDEP and nDEP cargo trapping mode (see Supplementary Video S3). The inset schematics in bright field images indicate the approximate location of transport of the micromotor with cargos within the entire chamber, while the yellow dotted circles indicate the location of the active carrier with cargos in the fluorescence field images. The bright and fluorescence field images were taken at similar times but with a small time difference of 1–3 s between them. White scale bar: 15 μm.

when compared to the functionalized beads (inset in Figure 4c).

Extension to More Complicated Microchannel Geometries. Such a simplified microchamber that does not necessitate any fabrication except drilled holes can be further complicated while still kept simple in terms of fabrication to include additional chambers if one, for example wishes, to perform multiplex (i.e., involving different functionalized beads), sandwich immunoassay, or several washing/buffer exchange/chemical reaction steps.[8,38−41] To prove the applicability of our generic micromotor-based functionalized cargo transport approach also to these potential future realizations of biosensing, we have fabricated a two-microchamber device with connecting microfluidic channel fabricated using direct laser cutting (Figure 5 and Supplementary Videos S5 and S6). It is clearly demonstrated that the JP can travel very long distances (through the connecting microchannel) while transporting cargo.

CONCLUSIONS

We have successfully demonstrated the ability to perform label-free and dynamic manipulation and transport of biotin-coated beads used as cargo via a JP acting as an active carrier. We have examined the ability to perform cargo loading under various solution conductivities including one (i.e., PBS) that is relevant for the binding of biotin-avidin. It was demonstrated that, using a single microfluidic chamber, simple and robust biosensing could be realized with the advantages of a micromotor-based approach avoiding the need for fluid handling as incubation time and washing steps can be simply controlled by moving the carrier itself. We have demonstrated the ability of transporting such a loaded carrier for very long distances through a microchannel connecting between two microchambers, which may be important for realizations of several buffer exchange/washing steps and/or multiplex sensing. This approach is applicable for a broad range of cargos from ∼100 nm size to several micrometer size. It is also possible to use a mixed population of cargos for multiplex biosensing where their loading/release can be controlled individually by taking advantage of their unique polarizability relative to the medium (i.e., Clausius−Mossotti factor) and the associated different crossover frequencies (COFs) at which the cargo switches between positive- and negative-DEP responses.[36]

Although examined for the biotin-avidin reaction, the approach is generic and can be applied for any antibody−

https://dx.doi.org/10.1021/acssensors.9b02041
ACS Sens. 2020, 5, 936−942

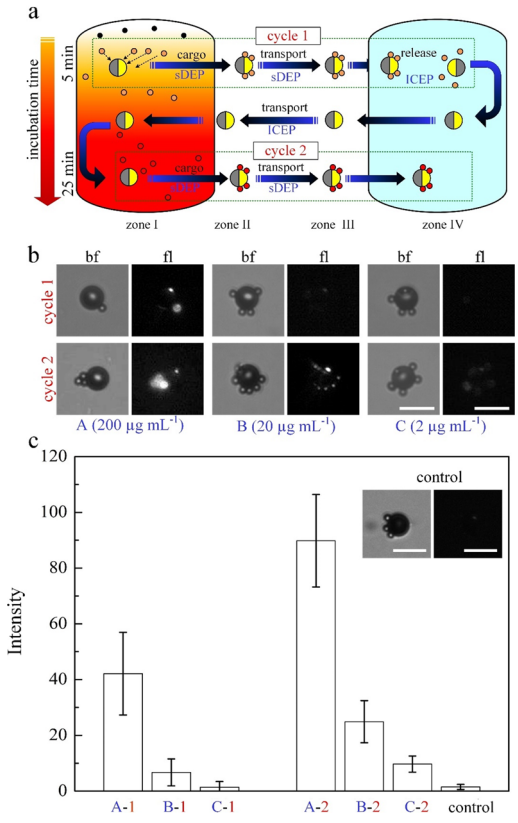

Figure 4. Several cycles of transport of biofunctionalized cargos within a single chamber system. (a) Schematics describing two cycles of cargo transport from zone I to zone IV (see Figure 3). The color change from orange to red indicates qualitatively the enhanced binding between avidin and biotin particles with increasing incubation time in zone I. After releasing the cargos at the end of the first cycle, the JP went back to zone I with propulsion mode of ICEP (10 kHz and 20 V_{PP}) to prevent loading cargos on the way (see Supplementary Video S4). The incubation times of avidin-biotin binding are 5 and 25 min at cycles 1 and 2, respectively. (b) Microscopy images of the transported cargo at zone IV with bright field and fluorescence mode for various initial avidin concentrations loaded at zone I. (c) Fluorescence intensity of avidin bound to biotin-coated cargos vs various initial avidin concentrations (A, B, and C) and two transport cycles (1 and 2). Microscopy images in the inset show non-biotin-coated beads (i.e., cargos) at zone IV under 200 μg mL^{-1} initial avidin concentration and 25 min incubation time as a control test. White scale bar: 15 μm.

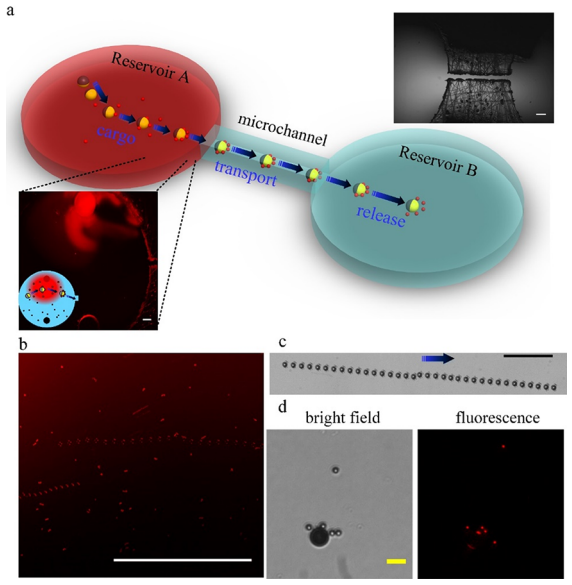

Figure 5. Transport of biotin-functionalized beads using a micromotor in a two chamber microfluidic system. (a) Schematics and a microscopy image of the microfluidic system (top right inset). In reservoir A, similarly to the format in Figure 3, the avidin molecules (200 μg mL^{-1}) are introduced into one of the inlet holes for binding biotin-functionalized particles for 20 min of incubation time. (b) Following incubation, a micromotor in reservoir A picks up avidin-bound biotin particles and transports them toward reservoir B. (c) Crossing the connecting microchannel (3.5 mm long) between the two reservoirs. The time interval between two superimposed images in b and c is 1 sec. The blue arrow indicates the direction of motion. (d) Bright field and fluorescence images of transported cargos at reservoir B. White, black, and yellow scale bars: 500, 100, and 10 μm, respectively.

antigen or DNA−probe combination. It can also be extended to include more microchambers for several reagents and washing steps as, for example, in a sandwich immunoassay where a reporting antibody is used for the fluorescence signal following the antigen binding to the antibodies immobilized on the surface of the cargos. Although we did not observe any significant effect of the binding on the DEP behavior of the cargos such that it necessitates tuning of the operating conditions, it is possible to easily tune the operating frequency if there is such an effect. The method is of particular use for low concentration of target analytes where the fast transportation of the carrier and trapped cargo toward the analyte region and away from it (i.e., washing step) enables fast detection that otherwise would be long due to the slow diffusion processes. Also, while we have demonstrated this using a single JP guided using magnetic steering so as to precisely control its translocation between the different regions and its incubation time within the region into which the analyte is introduced (region I), an operation mode where several such carriers are simultaneously operating autonomously (i.e., without magnetic steering) so as to enhance sampling of the analyte (i.e., reducing the otherwise long diffusion time) is also possible.

Due to the limitation of the electrokinetic propulsion to solution conductivities lower than ∼1 mS/cm, we chose, in the current study, a relatively low conductivity 0.01% (v/v) PBS solution at which the JP moves fast with sufficiently strong biotin-avidin binding affinity. However, since the cargo manipulation via DEP on the surface of the JP is valid also at physiological solutions of higher conductivity, it is only the propulsion mechanism that needs to be improved. One option is to replace the electrokinetic propulsion by other means, e.g., rotating magnetic field.[34,42] Another possible solutions may be to suppress the quenching of the EDL to higher solution conductivity by using highly ion-conductive polyelectrolyte coating.[43] We expect such a novel approach to open new opportunities in realizing simplified micromotor-based biosensing devices.

■ ASSOCIATED CONTENT

Supporting Information

The Supporting Information is available free of charge at https://pubs.acs.org/doi/10.1021/acssensors.9b02041.

Materials and methods, supplementary figures showing frequency dispersion of the Janus particle mobility

https://dx.doi.org/10.1021/acssensors.9b02041
ACS Sens. 2020, 5, 936−942

within solutions of higher conductivity, transition of cargo transport from sDEP with nDEP mode to ICEP with pDEP mode, cargo loading and transport using a 27 μm-diameter Janus particle micromotor, and supplementary video legends (PDF)

Supplementary Video S1, biotin-coated particles loading and transport by a single JP suspended in 0.01% diluted PBS under an applied electric field of 500 kHz and 20 V_{pp} (corresponds to Figure 2c) (MOV)

Supplementary Video S2, loading and transport of avidin-bound biotin cargos using a 27 μm-diameter Janus particle micromotor at a low frequency (20 kHz and 20 V_{pp}) under ICEP propulsion mode and nDEP trapping mode (corresponds to Figure S2) (MOV)

Supplementary Video S3, transport of biotin-functionalized cargos for sensing of avidin within a single chamber system under an applied field of 500 kHz and 20V_{pp} with magnetically directed motion (zones IV−I−IV) and incubation time of 5 min (corresponds to Figure 3) (MOV)

Supplementary Video S4, the transport of micromotor from zone IV to zone I under ICEP with nDEP mode (10 kHz and 20 V_{pp}) without trapping of biotin-functionalized beads (corresponds to Figure 4a) (MOV)

Supplementary Video S5, micromotor-based transport of avidin-bound, biotin-conjugated beads within reservoir A and toward the connecting microchannel under an applied field of 500 kHz and 20V_{pp} (corresponds to Figure 5b) (MOV)

Supplementary Video S6, micromotor-based transport of avidin-bound, biotin-conjugated beads through the long connecting microchannel (3.5 mm long) between the two reservoirs (corresponds to Figure 5c) (MOV)

Supplementary Video S7, manipulation of multiple JPs with magnetic steering (MOV)

AUTHOR INFORMATION

Corresponding Author

Gilad Yossifon − *Faculty of Mechanical Engineering, Micro- and Nanofluidics Laboratory, Technion−Israel Institute of Technology, Technion City 3200000, Israel;* orcid.org/0000-0001-7999-2919; Email: yossifon@technion.ac.il

Author

Sinwook Park − *Faculty of Mechanical Engineering, Micro- and Nanofluidics Laboratory, Technion−Israel Institute of Technology, Technion City 3200000, Israel*

Complete contact information is available at: https://pubs.acs.org/10.1021/acssensors.9b02041

Notes

The authors declare the following competing financial interest(s): We have submitted a patent describing the method.

ACKNOWLEDGMENTS

This work was supported by ISF grant 1938/16. Fabrication of the chip was made possible through the financial and technical support of the Russell Berrie Nanotechnology Institute and the Micro-Nano Fabrication Unit. We would like to acknowledge Eric Guyes and Prof. Matt Suss for assisting in laser fabrication of the two-chamber microfluidic device and Dr. Yue Wu for the technical assistance.

REFERENCES

(1) Sadik, O. A.; Van Emon, J. M. Applications of Electrochemical Immunosensors to Environmental Monitoring. *Biosens. Bioelectron.* **1996**, *11*, i−x.

(2) Xu, D.; Wang, Y.; Liang, C.; You, Y.; Sanchez, S.; Ma, X. Self-Propelled Micro/Nanomotors for On-Demand Biomedical Cargo Transportation. *Small* **2019**, *1902464*, 1902464.

(3) Kherzi, B.; Pumera, M. Self-Propelled Autonomous Nanomotors Meet Microfluidics. *Nanoscale* **2016**, *8*, 17415−17421.

(4) Xu, T.; Gao, W.; Xu, L. P.; Zhang, X.; Wang, S. Fuel-Free Synthetic Micro-/Nanomachines. *Adv. Mater.* **2017**, *29*, 1603250.

(5) Chen, C.; Soto, F.; Karshalev, E.; Li, J.; Wang, J. Hybrid Nanovehicles: One Machine, Two Engines. *Adv. Funct. Mater.* **2019**, *29*, 1806290.

(6) Sánchez, S.; Soler, L.; Katuri, J. Chemically Powered Micro- and Nanomotors. *Angew. Chem., Int. Ed.* **2015**, *54*, 1414−1444.

(7) Kong, L.; Guan, J.; Pumera, M. Micro- and Nanorobots Based Sensing and Biosensing. *Curr. Opin. Electrochem.* **2018**, *10*, 174−182.

(8) García, M.; Orozco, J.; Guix, M.; Gao, W.; Sattayasamitsathit, S.; Escarpa, A.; Merkoçi, A.; Wang, J. Micromotor-Based Lab-on-Chip Immunoassays. *Nanoscale* **2013**, *5*, 1325−1331.

(9) Sanchez, S.; Solovev, A. A.; Harazim, S. M.; Schmidt, O. G. Microbots Swimming in the Flowing Streams of Microfluidic Channels. *J. Am. Chem. Soc.* **2011**, *133*, 701−703.

(10) Baraban, L.; Tasinkevych, M.; Popescu, M. N.; Sanchez, S.; Dietrich, S.; Schmidt, O. G. Transport of Cargo by Catalytic Janus Micro-Motors. *Soft Matter* **2012**, *8*, 48−52.

(11) Brooks, A. M.; Tasinkevych, M.; Sabrina, S.; Velegol, D.; Sen, A.; Bishop, K. J. M. Shape-Directed Rotation of Homogeneous Micromotors via Catalytic Self-Electrophoresis. *Nat. Commun.* **2019**, *10*, 495.

(12) Mirin, N. A.; Halas, N. J. Light-Bending Nanoparticles. *Nano Lett.* **2009**, *9*, 1255−1259.

(13) Maggi, C.; Saglimbeni, F.; Dipalo, M.; De Angelis, F.; Di Leonardo, R. Micromotors with Asymmetric Shape That Efficiently Convert Light into Work by Thermocapillary Effects. *Nat. Commun.* **2015**, *6*, 7855.

(14) Wang, W.; Castro, L. A.; Hoyos, M.; Mallouk, T. E. Autonomous Motion of Metallic Microrods Propelled by Ultrasound. *ACS Nano* **2012**, *6*, 6122−6132.

(15) Sinn, I.; Kinnunen, P.; Pei, S. N.; Clarke, R.; McNaughton, B. H.; Kopelman, R. Magnetically Uniform and Tunable Janus Particles. *Appl. Phys. Lett.* **2011**, *98*, No. 024101.

(16) Fei, W.; Driscoll, M. M.; Chaikin, P. M.; Bishop, K. J. M. Magneto-Capillary Dynamics of Amphiphilic Janus Particles at Curved Liquid Interfaces. *Soft Matter* **2018**, *14*, 4661−4665.

(17) Gao, W.; Kagan, D.; Pak, O. S.; Clawson, C.; Campuzano, S.; Chuluun-Erdene, E.; Shipton, E.; Fullerton, E. E.; Zhang, L.; Lauga, E.; Wang, J. Cargo-Towing Fuel-Free Magnetic Nanoswimmers for Targeted Drug Delivery. *Small* **2012**, *8*, 460−467.

(18) Qiu, F.; Nelson, B. J. Magnetic Helical Micro- and Nanorobots: Toward Their Biomedical Applications. *Engineering* **2015**, *1*, 021−026.

(19) Boymelgreen, A.; Yossifon, G.; Miloh, T. Propulsion of Active Colloids by Self-Induced Field Gradients. *Langmuir* **2016**, *32*, 9540−9547.

(20) Boymelgreen, A. M.; Balli, T.; Miloh, T.; Yossifon, G. Active Colloids as Mobile Microelectrodes for Unified Label-Free Selective Cargo Transport. *Nat. Commun.* **2018**, *9*, 760.

(21) Han, K.; Shields, C. W., IV.; Velev, O. D. Engineering of Self-Propelling Microbots and Microdevices Powered by Magnetic and Electric Fields. *Adv. Funct. Mater.* **2018**, *28*, 1705953.

(22) Orozco, J.; Cortés, A.; Cheng, G.; Sattayasamitsathit, S.; Gao, W.; Feng, X.; Shen, Y.; Wang, J. Molecularly Imprinted Polymer-Based Catalytic Micromotors for Selective Protein Transport. *J. Am. Chem. Soc.* **2013**, *135*, 5336−5339.

(23) Delezuk, J. A. M.; Ramírez-Herrera, D. E.; de Ávila, B. E. F.; Wang, J. Chitosan-Based Water-Propelled Micromotors with Strong Antibacterial Activity. *Nanoscale* **2017**, *9*, 2195−2200.
(24) Wu, Z.; Li, J.; De Ávila, B. E. F.; Li, T.; Gao, W.; He, Q.; Zhang, L.; Wang, J. Water-Powered Cell-Mimicking Janus Micromotor. *Adv. Funct. Mater.* **2015**, *25*, 7497−7501.
(25) Morales-Narváez, E.; Guix, M.; Medina-Sánchez, M.; Mayorga-Martinez, C. C.; Merkoçi, A. Micromotor Enhanced Microarray Technology for Protein Detection. *Small* **2014**, *10*, 2542−2548.
(26) Esteban-Fernández De Ávila, B.; Martín, A.; Soto, F.; Lopez-Ramirez, M. A.; Campuzano, S.; Vásquez-Machado, G. M.; Gao, W.; Zhang, L.; Wang, J. Single Cell Real-Time MiRNAs Sensing Based on Nanomotors. *ACS Nano* **2015**, *9*, 6756−6764.
(27) Yan, J.; Han, M.; Zhang, J.; Xu, C.; Luijten, E.; Granick, S. Reconfiguring Active Particles by Electrostatic Imbalance. *Nat. Mater.* **2016**, *15*, 1095−1099.
(28) Lin, C. H.; Chen, Y. L.; Jiang, H. R. Orientation-Dependent Induced-Charge Electrophoresis of Magnetic Metal-Coated Janus Particles with Different Coating Thicknesses. *RSC Adv.* **2017**, *7*, 46118−46123.
(29) Squires, T. M.; Bazant, M. Z. Breaking Symmetries in Induced-Charge Electro-Osmosis and Electrophoresis. *J. Fluid Mech.* **2006**, *560*, 65−101.
(30) Gangwal, S.; Cayre, O. J.; Bazant, M. Z.; Velev, O. D. Induced-Charge Electrophoresis of Metallodielectric Particles. *Phys. Rev. Lett.* **2008**, *100*, No. 058302.
(31) Pethig, R. Review—Where Is Dielectrophoresis (DEP) Going? *J. Electrochem. Soc.* **2017**, *164*, B3049−B3055.
(32) Honegger, T.; Berton, K.; Picard, E.; Peyrade, D. Determination of Clausius-Mossotti Factors and Surface Capacitances for Colloidal Particles. *Appl. Phys. Lett.* **2011**, *98*, 181906.
(33) Jones, T. B. Liquid Dielectrophoresis on the Microscale. *J. Electrost.* **2001**, *51-52*, 290−299.
(34) Tottori, S.; Zhang, L.; Qiu, F.; Krawczyk, K. K.; Franco-Obregón, A.; Nelson, B. J. Magnetic Helical Micromachines: Fabrication, Controlled Swimming, and Cargo Transport. *Adv. Mater.* **2012**, *24*, 811−816.
(35) Demirörs, A. F.; Akan, M. T.; Poloni, E.; Studart, A. R. Active Cargo Transport with Janus Colloidal Shuttles Using Electric and Magnetic Fields. *Soft Matter* **2018**, *14*, 4741−4749.
(36) Huo, X.; Wu, Y.; Boymelgreen, A.; Yossifon, G. Analysis of Cargo Loading Modes and Capacity of an Electrically-Powered Active Carrier. *Langmuir* **2019**, DOI: 10.1021/acs.langmuir.9b03036.
(37) Wayment, J. R.; Harris, J. M. Biotin-Avidin Binding Kinetics Measured by Single-Molecule Imaging. *Anal. Chem.* **2009**, *81*, 336−342.
(38) Yasukawa, T.; Suzuki, M.; Sekiya, T.; Shiku, H.; Matsue, T. Flow Sandwich-Type Immunoassay in Microfluidic Devices Based on Negative Dielectrophoresis. *Biosens. Bioelectron.* **2007**, *22*, 2730−2736.
(39) Wagner, B.; Freer, H. Development of a Bead-Based Multiplex Assay for Simultaneous Quantification of Cytokines in Horses. *Vet. Immunol. Immunopathol.* **2009**, *127*, 242−248.
(40) Yu, X.; Hartmann, M.; Wang, Q.; Poetz, O.; Schneiderhan-Marra, N.; Stoll, D.; Kazmaier, C.; Joos, T. O. μFBI: A Microfluidic Bead-Based Immunoassay for Multiplexed Detection of Proteins from a μL Sample Volume. *PLoS One* **2010**, *5*, No. e13125.
(41) Kaewsaneha, C.; Tangboriboonrat, P.; Polpanich, D.; Eissa, M.; Elaissari, A. Janus Colloidal Particles: Preparation, Properties, and Biomedical Applications. *ACS Appl. Mater. Interfaces* **2013**, *5*, 1857−1869.
(42) Cui, J.; Huang, T. Y.; Luo, Z.; Testa, P.; Gu, H.; Chen, X. Z.; Nelson, B. J.; Heyderman, L. J. Nanomagnetic Encoding of Shape-Morphing Micromachines. *Nature* **2019**, *575*, 164−168.
(43) Zhan, X.; Wang, J.; Xiong, Z.; Zhang, X.; Zhou, Y.; Zheng, J.; Chen, J.; Feng, S. P.; Tang, J. Enhanced Ion Tolerance of Electrokinetic Locomotion in Polyelectrolyte-Coated Microswimmer. *Nat. Commun.* **2019**, *10*, 3921.

https://dx.doi.org/10.1021/acssensors.9b02041
ACS Sens. 2020, 5, 936−942